Nonclassical States of Cold Atomic Ensembles and of Light Fields

Academic and Research Staff
Professor Vladan Vuletic

Visiting Scientists and Research Affiliates
Dr. Saikat Ghosh, Dr. Sebastian Hofferberth, Dr. Fedja Orucevic

Graduate Students
Marko Cetina, Andrew Grier, Ian Leroux, Thibault Peyronel, Jonathan Simon, Monika Schleier-Smith, Haruka Tanji

Undergraduate Students
Wathid Assawasunthonnet, Benjamin Bloom, Amber Houghstow, Scott Morrison, Thaned Pruttivarasin, Adele Schwab

Support Staff
Joanna Keseberg

1. Heralded quantum memory for photon polarization states

Sponsors
National Science Foundation – Award ID number PHY 0555509
DARPA/ARO

A quantum memory [1,2,3], i.e. a device for storing and retrieving quantum states, is a key element of any quantum information processor. Optical memory access is highly desirable, since it is intrinsically fast, and single photons are robust, easily controlled carriers of quantum states. While a bit of quantum information (qubit) can be stored in a single two-level system, e.g. a single atom, it can be expedient to instead use long-lived collective spin excitations of an atomic ensemble. The ensemble can then be viewed as a “macro-atom" whose excitations are quantized spin waves (magnons), such that transitions between its energy levels (magnon number states) correspond to highly directional (superradiant) photon emission or absorption [4-12].

We have demonstrated a heralded quantum memory [3], i.e., system where a single photon announces polarization storage in the form of a single collective-spin excitation (magnon) that is shared between two spatially overlapped atomic ensembles. The heralded storage occurs rarely ($p \sim 10^{-6}$ in our non-optimized setup), but when it does, the incident photon is stored and can later be recreated with good efficiency ($\varepsilon \geq 50\%$) and sub-Poissonian statistics (g_2 = 0:24), while the photon polarization state is restored with very high fidelity (F > 90%).

Heralded storage is achieved by means of a spontaneous Raman process that simultaneously creates a photon of fixed polarization (that serves as the herald), and a magnon that is a copy of the input-beam polarization. To store an arbitrary polarization state

$$|\Psi\rangle = \sin\theta |R\rangle + e^{i\varphi} \cos\theta |L\rangle , \qquad (1)$$

written as a superposition of two right/left circularly polarized states $|R\rangle$, $|L\rangle$ with two arbitrary angles θ, φ, we use two spatially-overlapped atomic ensembles *A*, *B* inside an optical resonator (Fig. 1). The atomic levels are chosen such that ensemble *A* (*B*) absorbs only right (left) circularly polarized light, while both can emit a photon of the same polarization (π) into the resonator on the Raman transition of interest (Fig. 1). The detection of the emitted π photon heralds the mapping of the input polarization state onto a magnon, but does not provide “which-path" information to distinguish between *A* and *B*. The heralding also ensures that, even if the input is a coherent beam, only one magnon is generated between the two ensembles in the limit of small Raman

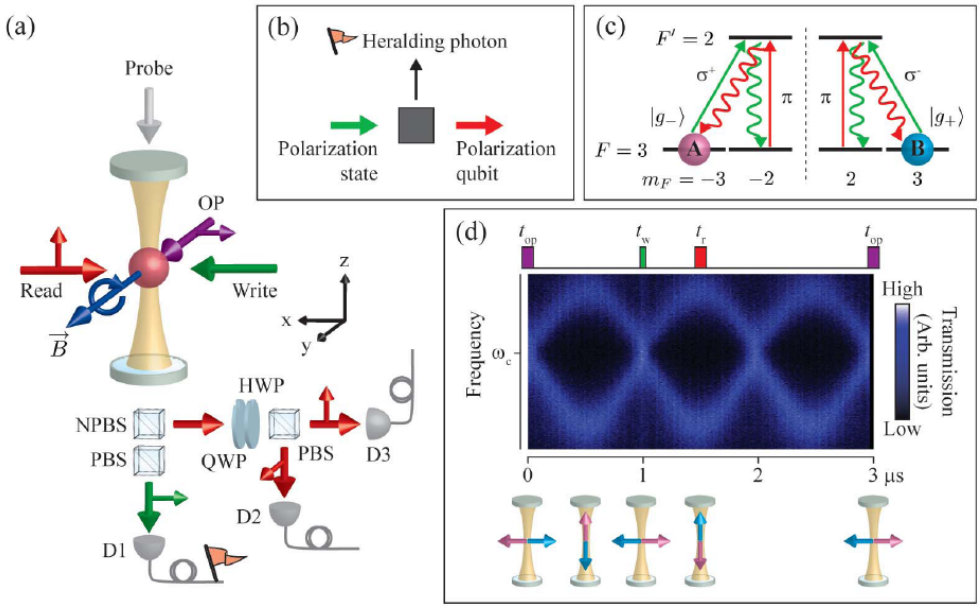

Figure 1. (a) Setup. Small arrows indicate beam polarization, OP is the optical pumping beam. NPBS, PBS, QWP, and HWP denote a non-polarizing beamsplitter, a polarizing beamsplitter, a quarter-waveplate, and a half-waveplate, respectively. D1, D2, D3 are single-photon counting modules. A static magnetic field produces magnon precession. **(b) Basic idea of the heralded storage.** A heralding photon of fixed polarization announces the storage of a photon of arbitrary, and potentially unknown polarization, in the atomic ensemble. **(c) Energy levels.** Ensembles *A* and *B* are initially prepared in $|g_{\pm}\rangle=|F=3,m_F=\pm 3\rangle$. The write (green) and the read (red) processes are $\sigma^{\pm}$–π and π– $\sigma^{\pm}$ spontaneous Raman transitions, respectively. **(d) Precession of the two macroscopic spins**, as measured by cavity transmission spectroscopy, and timing of the optical-pumping (t_{op}), write (t_w), and read (t_r) processes.

scattering probability. The "write" process thus projects the polarization state $|\psi\rangle$ onto a magnon superposition state

$$|\Phi\rangle \rightarrow |\Psi\rangle = \sin\theta\,|1\rangle_A|0\rangle_B + e^{i\varphi}\cos\theta\,|0\rangle_A|1\rangle_B\,, \qquad (2)$$

where $|n\rangle_k$ denotes *n* magnons in ensemble *k* (*k* = *A*, *B*). For general input polarization, this process creates an entangled state of the two ensembles. At a later time, the stored state can be retrieved on demand as a single photon by utilizing the strong coupling [4,12] of the magnon to the resonator mode ("read" process). The heralding serves to enhance the fidelity of the write process by announcing successful events. While the storage probability is low in our present setup, whenever there is a heralding event, a single magnon corresponding to the input-field polarization is stored with high fidelity. The single-photon nature of the retrieved field is confirmed by a conditional autocorrelation measurement indicating four-fold suppression of two-photon events compared to a Poissonian source (g_2 = 0.24(5)). The heralding process may thus be alternatively viewed as a quantum non-demolition measurement of a single photon which preserves the polarization, and stores the photon.

To investigate the quality of the heralded polarization memory, we evaluate the polarization fidelity of the retrieved single photon with respect to the input state. We determine the density matrix ρ_{meas} of the output polarization by measuring the projection onto three polarization bases: $2^{-1/2}(|R\rangle\pm|L\rangle)$ (H-V), $|R\rangle$ and $|L\rangle$ (L-R), and $2^{-1/2}(|R\rangle\pm i|L\rangle)$ (S-T). As the phase θ of the input state Eq. (1) is varied, the projection onto those bases displays a sinusoidal variation as expected (inset of Fig. 2). The polarization fidelities *F* of the retrieved single photons for the ten states

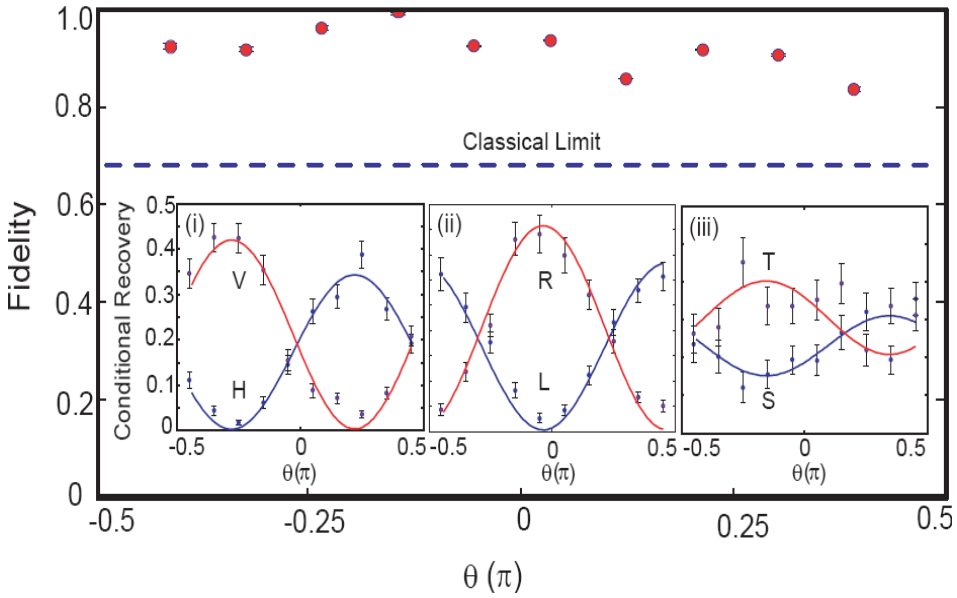

Figure 2. Polarization fidelity of the stored photon as a function of θ for φ=0 (Eq. 1). The dashed line indicates the classical limit of 2/3. Insets (i)-(iii): The results of projection measurements of the output field in three mutually-orthogonal bases, H-V, L-R, and S-T. The solid curves are a simultaneous fit for all sixty data points. The error bars represent statistical errors due to finite detection counts. No backgrounds have been subtracted.

shown in Fig. 2 as well as for the six fiducial input states, H, V, L, R, S, and T are evaluated from the measured density matrices. Fig. 2 shows that F is close to unity with no notable dependence on the zenith angle θ, and we have verified separately that the same is true for the azimuth angle φ. In particular, for any of the six fiducial states the measured fidelity *F* without any background subtraction is significantly above the classical limit of 2/3 for state-independent storage.

We also estimate the degree of entanglement present between samples *A* and *B* during storage. The amount of entanglement may be quantified by the concurrence *C* [14], where $1 \geq C > 0$ indicates entanglement. The concurrence of an atomic state C is bounded by that of the corresponding photonic state C_{ph} as discussed in the Supplementary Information of Ref. [13]. C_{ph} is observed to vary with zenith angle θ, as expected, with a maximum value of $C_{ph} = 0.034(4)$ for the $|H\rangle = 2^{-1/2}(|R\rangle + i|L\rangle)$ state.

The low success probability may be improved upon by a dipole trap and a modified resonator, which will realistically increase the transverse optical depth to unity, and the single-atom cooperativity in the cavity mode to 0.1, respectively. The success probability and the effective success rate will then be ~1% and ~200 s^{-1}, respectively. The retrieved photons in this scheme have controllable waveforms, and can easily be interfered with one another with high fringe contrast because of their narrow, nearly Fourier-limited bandwidth [10]. This is a crucial feature for any quantum information application. Furthermore, by applying this scheme to photons of undetermined polarization from a probabilistic source of entangled-photon pairs, it should be possible to realize a heralded source of high-quality entangled-photon pairs for various tasks in quantum information processing.

2. Generation of states with reduced quantum uncertainty for an atomic clock

Sponsors
DARPA
National Science Foundation – Award ID number PHY 0653414

Atomic clocks are the most accurate instruments ever developed. For clocks that operate with an atomic ensemble to improve the signal over that for a single particle, the precision is fundamentally limited by the projection noise associated with the uncorrelated random measurement outcomes for the individual particles [15-17], a situation referred to as the standard quantum limit (SQL). However, it is possible to induce quantum mechanical correlations (entanglement) between the particles to generate reduced-uncertainty states ("squeezed states") that overcome the SQL [18-20].

A two-level system can be formally described as a (pseudo-)spin s=1/2. In a typical precision experiment, the energy difference between the two levels is measured as a quantum mechanical phase accumulated in a given time. The result is read out as a population difference that can be formally viewed as the z-component S_z of the ensemble spin vector $\mathbf{S} = \sum \mathbf{s}_i$, where the sum is over the individual particles. The projection noise ΔS_z can be reduced by entanglement [16-19], by redistributing quantum noise from the S_z spin component to another spin component that is not directly affecting the experiment precision ("spin squeezing" [18-20]).

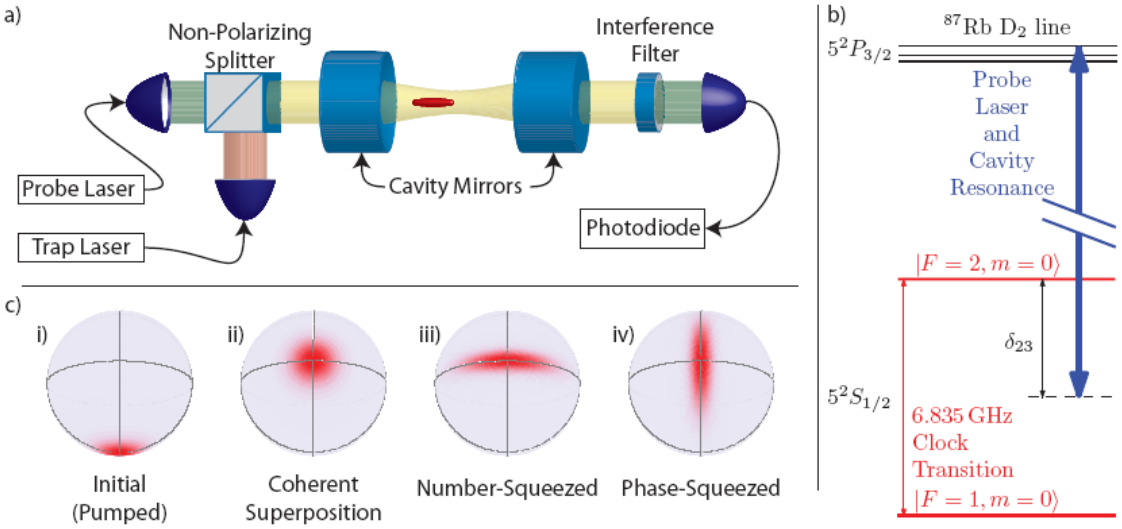

Figure 3. Measurement-induced pseudo-spin squeezing on an atomic clock transition. (a) Setup. A laser-cooled ensemble of ^{87}Rb atoms is loaded into a far-detuned optical dipole trap inside an optical resonator. The ensemble can be prepared in a superposition of hyperfine clock states $|1\rangle=|F=1,m_F=0\rangle$, $|2\rangle=|F=2,m_F=0\rangle$ by microwave pulses. A population difference N produces a resonator frequency shift that is measured with a probe laser. **(b) Atomic level structure.** The resonator is tuned such that atoms in the two clock states produce equal and opposite resonator frequency shifts via the state-dependent atomic index of refraction. **(c) Preparing a squeezed input state for an atomic clock.** A number-squeezed state (iii) can be generated from an unentangled state (coherent spin state, CSS) along x (ii) by measurement of N. It can then be rotated by a microwave pulse into a phase-squeezed state (iv), allowing a more precise determination of the phase acquired in the free evolution time of the atomic clock.

Spin squeezing requires an interaction between the particles [20] that can be achieved by collective coupling of the ensemble to a light field [21], provided the sample's optical depth (opacity if probed on resonance) is sufficiently large. Under appropriate conditions, the light-atom

interaction entangles the ensemble spin ***S*** with the electromagnetic field, and a subsequent field measurement can then project the atomic ensemble into a spin-squeezed state [16-21]. Such conditionally spin-squeezed input states can improve the sensitivity of a precision measurement device such as an atomic clock.

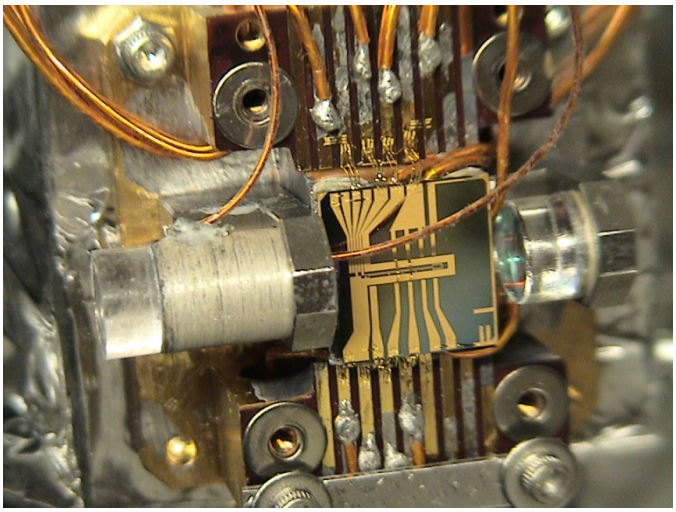

Figure 4. Microfabricated chip with mounted optical resonator. The resonator mode is aligned 200 μm above the surface of the microchip. The left mirror is mounted on a piezoceramic tube for tuning of the resonance frequency. The resonator finesse is F = 8000.

For an ensemble spin vector ***S*** oriented along the x axis, a state is spin squeezed [20] along the z-direction (or "number squeezed") if the uncertainty ΔS_z obeys $(\Delta S_z)^2 < |\langle S_x\rangle|/2$. For a maximally coherent system with $|\langle S_x\rangle| \approx S_0$, where $S_0 = N_0/2$ is the maximum possible spin of the ensemble containing N_0 particles, spin squeezing corresponds to a situation where the variance $(\Delta N)^2$ of the population difference $\Delta N = N_2 - N_1 = 2S_z$ between the two states $|1\rangle$, $|2\rangle$ is less than the projection noise limit, $(\Delta N)^2 < N_0$. However, since in real systems coherence (i.e. interference contrast) is often reduced, such that $|\langle S_x\rangle| < S_0$, spin-noise suppression below the projection noise limit $(\Delta S_z)^2 < |\langle S_x\rangle|/2$ is only a necessary but not a sufficient condition for spin squeezing. Thus to demonstrate spin squeezing one must measure both the spin noise ΔS_z, and the magnitude of the spin vector $|\boldsymbol{S}|$.

To prepare a spin-squeezed input state to an atomic clock, we adapt the proposal by Kuzmich, Bigelow, and Mandel [21] for a quantum non-demolition (QND) measurement of S_z with far off-resonant light [22]. An ensemble of up to 10^5 laser-cooled ^{87}Rb atoms is optically trapped inside an optical resonator that serves to enhance the signal and optical depth (Fig. 4). One resonator mode is tuned such that the state-dependent atomic index of refraction produces a mode frequency shift that is proportional to the population difference $N = N_2 - N_1 = 2S_z$ between the hyperfine clock states $|1\rangle = |5S_{1/2},F=1,m_F=0\rangle$ and $|2\rangle = |5S_{1/2},F=2,m_F=0\rangle$. Then a QND measurement of S_z can be performed by measuring the transmission of a weak probe beam through the ensemble-resonator system. A frequency stabilization system for probe laser and resonator ensures that the probe transmission noise is close to the photocurrent shot-noise limit.

Fig. 5 shows the projection noise for an unentangled state of uncorrelated atoms (coherent spin state, CSS), and the quantum noise for a conditionally prepared entangled state with a random, but known value of S_z. For the former (red data points) the linear dependence of $(\Delta S_z)^2$ on total atom number N_0 shows that we have prepared a state at the projection noise limit. For the latter, at low atom number the measurement noise exceeds the SQL due to photon shot noise and

some technical noise (dash-dotted green line in Fig. 2), while at higher atom number $N_0 = 3\times10^4$ we achieve a 9 dB suppression of spin noise below the SQL.

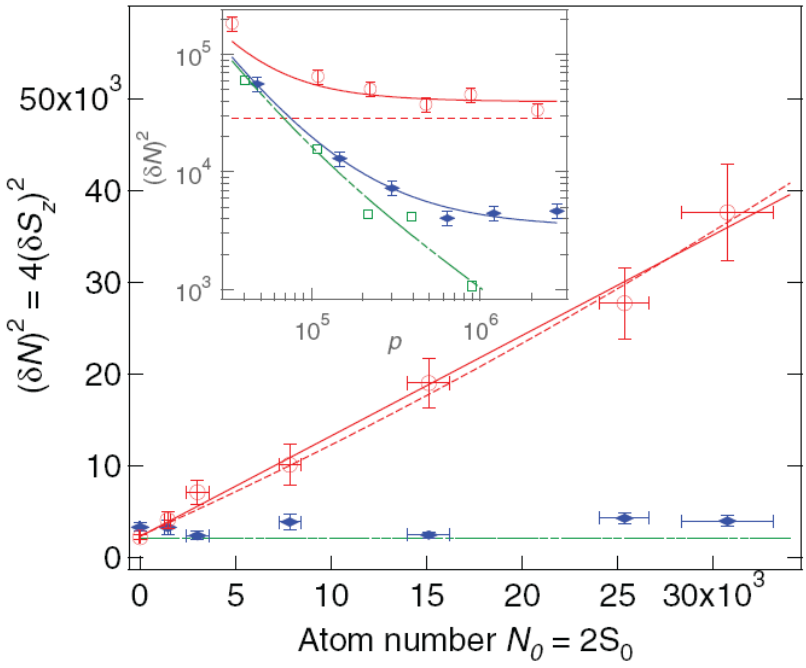

Figure 5. Projection noise limit and spin noise reduction. The measured spin noise for an uncorrelated state (CSS, open red circles) agrees with the theoretical prediction $(\Delta S_z)^2=S_0/2$, with negligible technical noise (solid and dashed red lines). Our measurement of S_z at photon number $p=5\times10^5$ has an uncertainty $(\delta S_z)^2$ (solid blue diamonds) substantially below the SQL. Inset: Dependence of spin measurement $(\delta S_z)^2=(\delta N)^2/4$ on probe photon number p for $N_0=3\times10^4$. With increasing photon number, the measurement uncertainty (solid blue diamonds) drops below the projection noise level (dashed red line). Also shown is the technical noise without atoms expressed as an equivalent spin noise (open green squares).

The reduction of ΔS_z below the SQL is accompanied by a substantial increase in ΔS_y. The shape of the uncertainty region can be verified by rotating the state prepared by the squeezing pulse by a variable angle about $\langle \boldsymbol{S} \rangle$ before performing the second S_z measurement. The variance $(\Delta S_\alpha)^2$ thus obtained is displayed in Fig. 6. The data are well described by a model that assumes the spin noise after the first measurement to constitute an ellipse with its short axis along *z* (solid blue line). The uncertainty area $A = \Delta S_z \Delta S_y$ is well above the Heisenberg limit $A_H = |\boldsymbol{S}|/2$ (dashed green line). The larger uncertainty is primarily due to the atomic-projection-noise-induced resonator shift, which produces fluctuations in probe transmission well above the photon shot noise limit, resulting in substantial differential light shifts between the clock states. This effect, though not currently a limitation on our squeezing performance, can be reduced in future experiments by measuring on cavity resonance, or by using a feedback technique that keeps the transmitted photon number constant.

When we compare the observed squeezing to the reduction of clock signal $|\boldsymbol{S}|$, measured via the clock fringe contrast, we find that we achieve 4dB of spin squeezing [20], and 3dB of improvement in clock signal-to-noise ratio over the standard quantum limit [16,17]. The contrast loss is not fundamental, and in part simply limited by the detuning and intensity of the light used to stabilize the resonator length. We are currently making modifications to the setup to reduce this technical noise. If successful, the improvement in signal-to-noise ratio should allow us to obtain an improvement over the SQL that matches the observed spin noise reduction of 9dB. If technical noise can be suppressed further, a fundamental limit associated with scattering into free space is

set by the optical depth OD of the sample [19], which for our present parameters (OD ≈ 5×10^3) would amount to ~18 dB of spin squeezing.

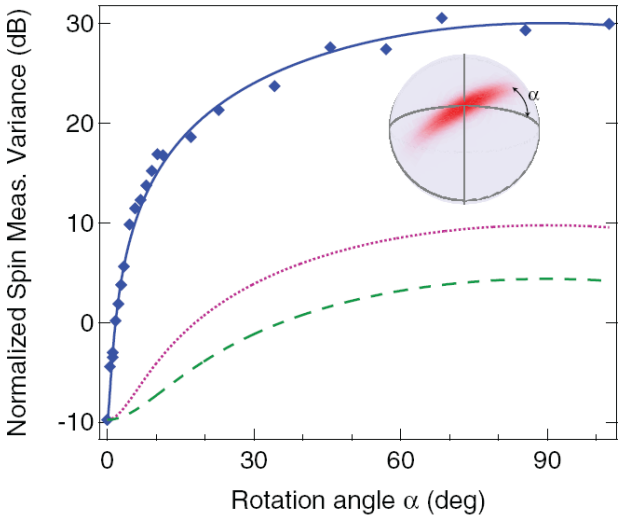

Figure 6. Shape of the squeezed uncertainty region. A rotation about the mean spin vector $\langle \boldsymbol{S} \rangle$ is applied between the first and second spin measurements. The spin noise reduction along z (α=0) below the projection noise limit is accompanied by a substantial spin noise increase in the equatorial plane ($\alpha=\pi/2$). The solid blue line corresponds to an elliptic shape of the uncertainty region. The dotted magenta line would correspond to a state at the Heisenberg limit in the ideal case where the measurement does not reduce the length of the spin vector $|\boldsymbol{S}|$. The dashed green line is the true Heisenberg limit for our measurement, taking into account the reduction of $|\boldsymbol{S}|$.

3. Cold collisions between trapped ions and trapped atoms

Sponsors
DARPA
National Science Foundation – Award ID number PHY 0653414

Studies of cold collisions between trapped neutral atoms have revealed a multitude of interesting quantum phenomena, including Wigner threshold laws, magnetically tunable Feshbach resonances, controlled molecule formation, and the suppression of individual scattering channels (see Ref. [23] for references). Collisions between trapped ions, on the other hand, are featureless, since the strong long-range repulsive Coulomb interaction prevents the ions from approaching each other. Collisions between ions and neutral atoms [24-27], of interest to atmospheric and interstellar science [27-29], fall into an intermediate regime where an attractive long-range r^{-4} potential leads to semiclassical behavior for a wide range of collision energies, but where quantum phenomena dominate collisions at very low energies. Cold ion-atom collisions have been proposed as a means to demonstrate quantum gates [30], to cool atoms [31] or molecules [27,32,33] lacking closed optical transitions, or to bind small Bose-Einstein condensates to an ion [34]. However, there has been little experimental work, and all previous studies have used free (i.e. hot) ions and/or hot atoms [28,29,35].

The long-range interaction potential between a singly charged ion and a neutral atom is the energy of the induced atomic dipole in the ion's electric field, given by $V(r) = -C_4/(2r^4)$, where $C_4=\alpha q^2/(4\pi\varepsilon_0)^2$ is proportional to the atomic polarizability α, and q is the electron charge. For given collision energy E in the center-of-mass frame, there is a critical impact parameter

$b_c=(2C_4/E)^{1/4}$ which separates two types of collisions: those with impact parameter $b<b_c$ that result in inward-spiraling orbits of radius approaching zero, and those with $b>b_c$ that never cross the

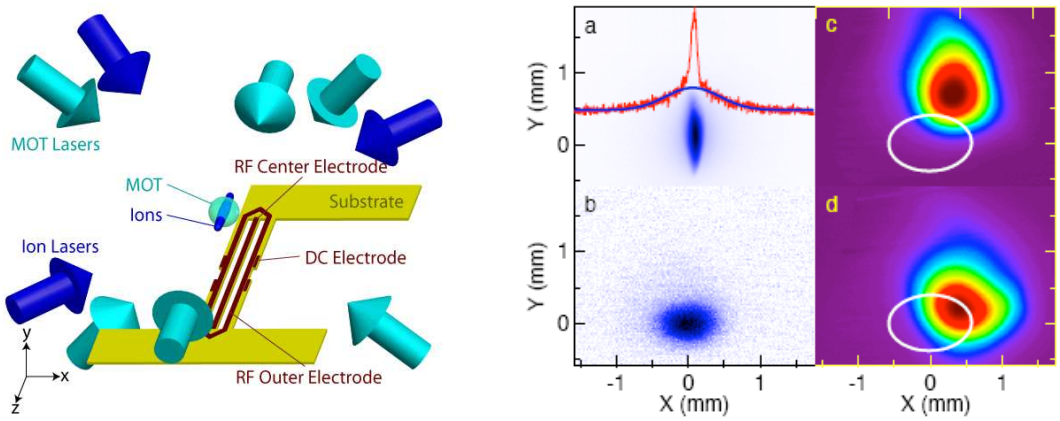

Figure 7. *Left*: **Setup for trapping neutral (MOT) and singly charged (surface planar Paul trap) Yb in the same spatial volume.** The MOT can be moved in all three directions by adjusting the local magnetic field. The ion trap can be moved vertically by adjusting the ratio of voltages applied to the central and outer rf electrodes. Stray dc field compensation and trapping along *z* is provided by dc electrodes. *Right*: **(a) Secondary camera image of the ion crystal** (blue) and cross-section showing highly non-Gaussian shape of crystal (red). (b) Primary camera image of the ion crystal. (c) Typical low-overlap setting between MOT (colored contours) and $1/e^2$ contour of ions (white). (d) Same as (c) but for a large overlap setting.

angular-momentum barrier [18,20], and where the distance of closest approach exceeds $b_c/2^{1/2}$. For a resonant charge-exchange collision $A^+ + A \rightarrow A + A^+$ of an ion with its parent atom, a semiclassical cross section σ_{ce} can be simply derived, provided that b_c is large compared to the range r_0 of the molecular potential: For collisions with $b>b_c$ the electron should remain bound to the incoming atom, while for inward-spiraling collisions with $b<b_c$ the electron should with equal probability attach to either nucleus. It follows that the charge-exchange cross section is $\sigma_{ce}=\sigma_L/2$, where $\sigma_L = \pi b_c^2 = \pi\sqrt{2C_4/E}$ is the Langevin cross section [36]. The corresponding rate coefficient $K = \sigma_L v = \pi\sqrt{C_4/\mu}$, where v is the relative particle velocity and μ the reduced mass, is independent of energy. This Langevin regime is valid over many orders of magnitude in collision energy.

We use a magneto-optical trap (MOT) in combination with a Paul trap, as originally proposed by W. Smith [31], to study Yb^++Yb collisions [38]. The setup is described in detail in Ref. [37], and depicted in Fig. 7. In the present work, ^{172}Yb, ^{174}Yb, or ^{171}Yb atoms are loaded from a beam into a MOT resonant with the $^1S_0 \rightarrow {}^1P_1$ transition in neutral Yb at λ = 398.8 nm. Typically, the MOT contains 3×10^5 atoms at a peak density of 2×10^8 cm^{-3}, and an estimated temperature of 1 mK.

Cold ions are produced by photoionization from the excited state $^1P_1$ of the MOT with 370-nm laser light [37]. The ion trap is a surface-electrode Paul trap commercially printed on a vacuum-compatible substrate consisting of three, 18 μm-thick, 1-mm-wide copper rf electrodes and twelve dc-compensation electrodes. The trap is typically operated at 1.4 MHz with amplitude of 520 V on the outer electrodes and -460 V on the inner electrode. This creates a 0.3 eV deep pseudo-potential trap 3.6 mm above the trap surface with a secular frequency of 67 kHz. Ion trap populations can be adjusted between a single and 10^4 ions by varying the trap loading time.

In our system, charge-exchange collisions between different isotopes can be directly observed via the isotope-selective ion fluorescence: we first load the ion trap from the MOT with one isotope, change the MOT isotope by adjusting the frequency of the 399-nm laser, and then monitor the decay of the ion population through the decay of the 370-nm fluorescence. Without

the MOT, the ion trap loss is exponential with a typical lifetime of τ=400 s (Fig. 2, red circles) for ion crystals. In the presence of the MOT, τ is substantially shortened, with a shorter lifetime for higher MOT density (blue squares and green triangles).

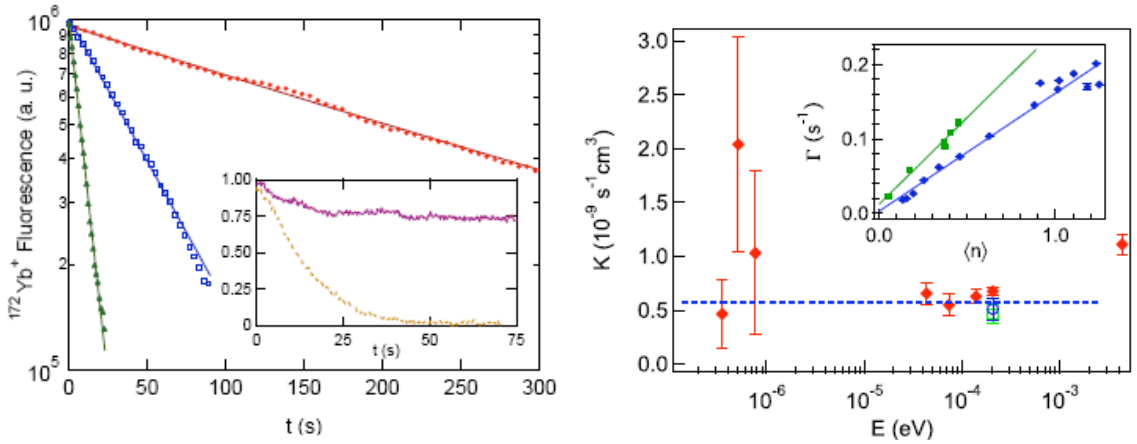

Figure 8. *Left*: **Typical ^{172}Yb$^+$ ion-crystal fluorescence decay** and exponential fits for no (red circles) moderate (blue squares), and high (green triangles) ^{174}Yb atomic density at the ion trap site. *Right*: **Charge-exchange rate coefficient *K*** as a function of collision energy *E*. Diamonds (red) are ^{172}Yb$^+$+^{174}Yb, the circle (blue) ^{172}Yb$^+$+^{171}Yb, and the square (green) ^{174}Yb$^+$+^{172}Yb. Dashed line (blue) corresponds to one half the Langevin rate coefficient calculated using the value α=143 a.u. for the Yb atomic polarizability. The three data points at the lowest collision energies were measured with single ions, all others with larger ion crystals, leading to reduced statistical uncertainty. Inset: Decay rate constant Γ as a function of ^{174}Yb density $\langle n \rangle$ in units of 10^8 cm^{-3} seen by ^{172}Yb$^+$ for collision energies of 210 eV (blue diamonds) and 4.4 meV (green squares).

To accurately determine σ_{ce}, we vary the atomic density as seen by the ions by moving the MOT with a magnetic bias field that displaces the zero of the MOT quadrupole field. We determine the local atomic density as seen by the ions by taking images of both the MOT cloud and the ions on a charge-coupled device (CCD) camera (see Fig. 7), with the total atom number calibrated with a resonant-absorption measurement. The rate coefficient plotted against collision energy is shown in Fig. 8. The three data points at lowest energies, within a factor of six of the Doppler-limited temperature, were taken with single ions as the energy of two ions displaced along the radial direction is already on the order of 10 μeV. The other points were taken with up to a few thousand ions, and consequently have smaller statistical uncertainties. Except for the highest-energy point at E = 4 meV, the inelastic rate coefficient is independent of E over the full range of energies investigated here.

Using the ab initio value of polarizability α = 143 a.u. [27], we calculate a inelastic Langevin rate coefficient K_{th}=5.8×10^{-10} cm^3 s^{-1}, in agreement with our experimentally measured value of K_{exp} =6×10^{-10} cm^3 s^{-1}. We estimate that the accuracy of the latter to be 50% due to the uncertainty in absolute MOT atom number calibration. As shown in Fig. 8, this value for K was observed for all isotope combinations investigated here: ^{172}Yb$^+$ +^{174}Yb, ^{174}Yb$^+$ +^{172}Yb, and ^{174}Yb$^+$ +^{171}Yb. The fact that we observe no deviation from the Langevin law, and the same value for the scattering cross section for ^{172}Yb$^+$ +^{174}Yb and ^{174}Yb$^+$ +^{172}Yb even at the lowest collision energies, can be used to constrain the difference in ionization energies of the two isotopes to less than 400 neV, or 6 parts in 10^8 of the Yb ionization energy of 6.25416 eV [28].

All the Yb isotopes used in this experiment have been cooled to quantum degeneracy in an optical dipole trap [39,40], which would allow the investigation of collision processes between an ion and a Bose-Einstein condensate [34] or Fermi sea. Alternatively, to avoid the large resonant

charge-exchange cross section observed here, a different species such as Rb could be used for sympathetic cooling of ions or for studying ion impurities in a Bose-Einstein condensate.

References

[1] D.N. Matsukevich and A. Kuzmich, “Quantum State Transfer Between Matter and Light,” Science **306**, 663-666 (2004).

[2] K.S. Choi and H. Deng and J. Laurat and H.J. Kimble, “Mapping photonic entanglement into and out of a quantum memory,” Nature **452**, 67-71 (2008).

[3] H. Tanji, S. Ghosh, J. Simon, B. Bloom, and V. Vuletic, “Heralded single-magnon quantum memory for photon polarization states,” submitted to Phys. Rev. Lett. (8/2008), quant-ph/0808.3603.

[4] L.-M. Duan, M. D. Lukin, J. I. Cirac, and P. Zoller, “Generation of nonclassical photon pairs for scalable quantum communication with atomic ensembles”, Nature **414**, 413 (2001).

[5] Kuzmich, W. P. Bowen, A. D. Boozer, A. Boca, C. W. Chou, L.-M. Duan, and H. J. Kimble, “Generation of nonclassical photon pairs for scalable quantum communication with atomic ensembles”, Nature **423**, 731 (2003).

[6] H. van der Wal, M. D. Eisaman, A. Andre, R. L. Walsworth, D. F. Phillips, A. S. Zibrov, and M. D. Lukin, “Atomic Memory for Correlated Photon States”, Science **301**, 196 (2003).

[7] C. W. Chou, H. de Riedmatten, D. Felinto, S. V. Polyakov, S. J. van Enk and H. J. Kimble, ”Measurement-induced entanglement for excitation stored in remote atomic ensembles”, Nature **438**, 828 (2005).

[8] T. Chanelière, D. N. Matsukevich, S. D. Jenkins, S.-Y. Lan, T. A. B. Kennedy and A. Kuzmich, ”Storage and retrieval of single photons transmitted between remote quantum memories”, Nature **438**, 833 (2005).

[9] M. D. Eisaman, A. André, F. Massou, M. Fleischhauer, A. S. Zibrov and M. D. Lukin, ”Electromagnetically induced transparency with tunable single-photon pulses”, Nature **438**, 837 (2005).

[10] J. K. Thompson, J. Simon, H. Loh, and V. Vuletic, “A High-Brightness Source of Narrowband, Identical-Photon Pairs,” Science **303**, 74-77 (2006).

[11] A.T. Black, J. K. Thompson, and V. Vuletic, “On-Demand Superradiant Conversion of Atomic Spin Gratings into Single Photons with High Efficiency,” Phys. Rev. Lett. **95**, 33601 (1-4) (2005).

[12] J. Simon, H. Tanji, J. K. Thompson, and V. Vuletic, “Interfacing Collective Atomic Excitations and Single Photons,” Phys. Rev. Lett. **98**, 183601 (1-4) (2007).

[13] J. Simon, H. Tanji, S. Ghosh, and V. Vuletic, “Single-Photon Bus between Spin-Wave Quantum Memories,” Nature Physics **3**, 765-769 (2007).

[14] W. K. Wootters, “Entanglement of Formation of an Arbitrary State of Two Qubits," Phys. Rev. Lett. **80**, 2245-2248 (1998).

[15] G. Santarelli, Ph. Laurent, P. Lemonde, A. Clairon, A. G. Mann, S. Chang, A. N. Luiten, and C. Salomon, “Quantum Projection Noise in an Atomic Fountain: A High Stability Cesium Frequency Standard," Phys. Rev. Lett. **82**, 4619-4622 (1999).

[16] D. J. Wineland, J. J. Bollinger, W. M. Itano, F. L. Moore, D. J. Heinzen, “Spin squeezing and reduced quantum noise in spectroscopy,” Phys. Rev. A **46**, R6797 (1992).

[17] D. J. Wineland, J. J. Bollinger, W. M. Itano, D. J. Heinzen, “Squeezed atomic states and projection noise in spectroscopy,” Phys. Rev. A **50**, R67 (1994).

[18] V. Meyer, M. A. Rowe, D. Kielpinski, C. A. Sackett, W. M. Itano, C. Monroe, and D. J. Wineland, “Experimental Demonstration of Entanglement-Enhanced Rotation Angle Estimation Using Trapped Ions," Phys. Rev. Lett. **86**, 5870-5873 (2001).

[19] D. Leibfried, M.D. Barrett, T. Schaetz, J. Britton, J. Chiaverini, W.M. Itano, J.D. Jost, C. Langer, and D. Wineland, “Toward Heisenberg-Limited Spectroscopy with Multiparticle Entangled States," Science **304**, 1476 (2004).

[20] M. Kitagawa and M. Ueda, “Squeezed spin states,” Phys. Rev. A **47**, 5138 (1993).

[21] A. Kuzmich, N. P. Bigelow, and L. Mandel, “Atomic quantum non-demolition measurements and squeezing,” Europhys. Lett. **42**, 481-486 (1998).

[22] A. Kuzmich, L. Mandel, N. P. Bigelow, “Generation of Spin Squeezing via Continuous Quantum Nondemolition Measurement,” Phys. Rev. Lett. **85**, 1594-1597 (2000).

[23] T. Kohler, K. Goral, and P. S. Julienne, “Production of cold molecules via magnetically tunable Feshbach resonances,” Rev. Mod. Phys. **78**, 1311 (2006).

[24] R. Cote and A. Dalgarno, “Ultracold atom-ion collisions,” Phys. Rev. A **62**, 012709 (2000).

[25] O. Makarov, R. Cote, H. Michels, and W. W. Smith, “Radiative charge-transfer lifetime of the excited state of $NaCa^+$,” Phys. Rev. A **67**, 042705 (2003).

[26] Z. Idziaszek, T. Calarco, P. S. Julienne, and A. Simoni, “Quantum theory of ultracold atom-ion collisions,” atom-phys/0806.4002 (2008).

[27] K. Mølhave and M. Drewsen, “Formation of translationally cold MgH^+ and MgD^+ molecules in an ion trap,” Phys. Rev. A **62**, 011401 (2000).

[28] T. Speck, T. I. Mostefaoui, D. Travers, and B. R. Rowe, “Pulsed injection of ions into the CRESU experiment,” Int. J. Mass Spectrom. **208**, 73 (2001).

[29] V. H. S. Kwong, D. Chen, and Z. Fang, “Dissociative charge transfer between ground-state He^+ and CO at electron-volt energies,” Astrophys. J. **536**, 954 (2000).

[30] Z. Idziaszek, T. Calarco, and P. Zoller, “Controlled collisions of a single atom and an ion guided by movable trapping potentials,” Phys. Rev. A **76**, 033409 (2007).

[31] W. W. Smith, O. P. Makarov, and J. Lin, “Cold ion-neutral collisions in a hybrid trap,” J. Mod. Opt. **52**, 2253 (2005).

[32] Y. Moriwaki, M. Tachikawa, Y. Maeno, and T. Shimizu, “Collision Cooling of Ions Stored in Quadrupole Radio-Frequency Trap,” Jpn. J. Appl. Phys. **31**, 1640 (1992).

[33] O. P. Makarov, R. Cote, H. Michels, and W. W. Smith, "Radiative charge-transfer lifetime of the excited state of $NaCa^{+}$," Phys. Rev. A **67**, 042705 (2003).

[34] R. Cote, V. Kharchenko, and M. D. Lukin, "Mesoscopic Molecular Ions in Bose-Einstein Condensates," Phys. Rev. Lett. **89**, 093001 (2002).

[35] P. F. Staanum, K. Højberre, R. Wester, and M. Drewsen, atom-phys/0802.2797 (2008).

[36] P. Langevin, Ann. Chim. Phys. **5**, 245 (1905).

[37] M. Cetina, A. Grier, J. Campbell, I. Chuang, and V. Vuletic, Phys. Rev. A **76**, 041401 (2007).

[38] "Observation of Cold Charge-Exchange Collisions between Trapped Ions and Trapped Atoms," A. Grier, M. Cetina, F. Orucevic, and V. Vuletic, submitted to Phys. Rev. Lett. (8/2008), physics.atom-ph/0808.3620.

[39] Y. Takasu, K. Maki, K. Komori, T. Takano, K. Honda, M. Kumakura, T. Yabuzaki, and Y. Takahashi, Phys. Rev. Lett. **91**, 040404 (2003).

[40] T. Fukuhara, Y. Takasu, M. Kumakura, and Y. Takahashi, Phys. Rev. Lett. **98**, 030401 (2007).

Publications

1. Journal Articles

Published:

"Single-Photon Bus between Spin-Wave Quantum Memories," J. Simon, H. Tanji, S. Ghosh, and V. Vuletic, Nature Physics **3**, 765-769 (2007).

"Bright Source of Cold Ions for Surface-Electrode Traps," M. Cetina, A. Grier, J. Campbell, I. Chuang, and V. Vuletic, Phys. Rev. A **76**, 041401(R) (2007).

Submitted for publication:

"Generating Reduced-Quantum-Uncertainty States for an Atomic Clock," M. H. Schleier-Smith, I.D. Leroux, and V. Vuletic, submitted to Science (8/2008).

"Observation of Cold Charge-Exchange Collisions between Trapped Ions and Trapped Atoms," A. Grier, M. Cetina, F. Orucevic, and V. Vuletic, submitted to Phys. Rev. Lett. (8/2008), physics.atom-ph/0808.3620.

"Heralded single-magnon quantum memory for photon polarization states," H. Tanji, S. Ghosh, J. Simon, B. Bloom, and V. Vuletic, submitted to Phys. Rev. Lett. (8/2008), quant-ph/0808.3603.

"Few-photon switching within a fiber-optical system," M.Bajcsy, S. Hofferberth, V. Balic, T. Peyronel, A.S. Zibrov, V. Vuletic, and M.Lukin, submitted to Nature (8/2008).

"Crystallization of strongly interacting photons in a nonlinear optical fiber," D.E. Chang, V. Gritsev, G. Morigi, V. Vuletic, M.D. Lukin, and E. Demler, accepted into Nature Physics (7/2008).

Meeting Papers

"Spin Squeezing on an Atomic-Clock Transition," M. H. Schleier-Smith, I.D. Leroux, and V. Vuletic, XXI. International Conference on Atomic Physics (ICAP 2008, University of Connecticut, Storrs, 8/2008).

"Entanglement for atomic clocks beyond the standard quantum limit," M. H. Schleier-Smith, I.D. Leroux, and V. Vuletic, Colloquium of the Institute for Physics, Belgrade, Serbia (6/2008).

"Single-Photon Bus between Spin-Wave Quantum Memories," J. Simon, H. Tanji, S. Ghosh, and V. Vuletic, Colloquium of the Max-Planck Institute for Quantum Optics, Garching, Germany (6/2008).

"Generation and Quantum Storage of Single Photons," J. Simon, H. Tanji, S. Ghosh, and V. Vuletic, 15th Central European Workshop on Quantum Optics, Belgrade, Serbia (5/2008).

"Generation and Quantum Storage of Single Photons," J. Simon, H. Tanji, S. Ghosh, and V. Vuletic, Physics Colloquium, University of Massachusetts Lowell (10/2007).

"Observation of cold collisions between trapped ions and trapped atoms," M. Cetina, A. Grier, F. Orucevic, and V. Vuletic, Atomic Physics Seminar, University of Connecticut, (10/2007).

"Photonic bus connecting atomic-ensemble spin-wave quantum memories," J. Simon, H. Tanji, S. Ghosh, and V. Vuletic, talk given by S. Ghosh, OSA Annual Meeting (Frontier in Optics 2007), (San Jose 9/2007)

"Photon sources for quantum information processing," V. Vuletic, Atomic Physics Gordon Research Conference (Tilton 7/2007).

"Microchips for single atom detection and spin squeezing," M. Schleier-Smith, I. Leroux, I. Teper, Y. Lin, and V. Vuletic, talk given by I. Teper, IQEC/CLEO-PR2007 (Munich 6/2007).